Chemistry–A European Journal
Research Article
doi.org/10.1002/chem.202201731
Chemistry Europe
European Chemical Societies Publishing
www.chemeurj.org

Solvent Effects on Ultrafast Charge Transfer Population: Insights from the Quantum Dynamics of Guanine-Cytosine in Chloroform

James A. Green,*[a] Sandra Gómez,[b, c] Graham Worth,[b] Fabrizio Santoro,*[d] and Roberto Improta*[a]

Abstract: We study the ultrafast photoactivated dynamics of the hydrogen bonded dimer Guanine-Cytosine in chloroform solution, focusing on the population of the Guanine→Cytosine charge transfer state (GC-CT), an important elementary process for the photophysics and photochemistry of nucleic acids. We integrate a quantum dynamics propagation scheme, based on a linear vibronic model parameterized through time dependent density functional theory calculations, with four different solvation models, either implicit or explicit. On average, after 50 fs, 30~40% of the bright excited state population has been transferred to GC-CT. This process is thus fast and effective, especially when transferring from the Guanine bright excited states, in line with the available experimental studies. Independent of the adopted solvation model, the population of GC-CT is however disfavoured in solution with respect to the gas phase. We show that dynamical solvation effects are responsible for this puzzling result and assess the different chemical-physical effects modulating the population of CT states on the ultrafast timescale. We also propose some simple analyses to predict how solvent can affect the population transfer between bright and CT states, showing that the effect of the solute/solvent electrostatic interactions on the energy of the CT state can provide a rather reliable indication of its possible population.

Introduction

The population of excited electronic states with significant charge transfer (CT) character is a key step of many processes of huge biological and technological interest, from DNA photodamage/protection to photosynthesis and solar energy conversion.[1–12] In order to fully understand, and ultimately master these processes, assessing the chemical physical effects ruling the population of CT states starting from the 'spectroscopic' bright excited state(s) is thus very important. This is a challenging task as it is necessary to accurately describe the interplay between several close-lying excited electronic states of at least two different chromophores, requiring a proper inclusion of vibronic effects, possibly at a full quantum level. Moreover, almost all the biological and industrial photoactivated processes occur in the condensed phase, and thus the treatment of solvation effects is mandatory.

In this manuscript, we focus on this latter aspect and use quantum dynamical (QD) simulations to study the interplay between bright and CT states in the hydrogen bonded dimer formed in chloroform by two derivatives of guanosine (G) and cytidine (C) in a Watson-Crick (WC) arrangement. This process has a significant biological relevance, since it has been proposed to provide an effective excited state decay route for the photoexcited state population of the GC pair, triggering an intermolecular proton transfer (PT), the so-called proton coupled electron transfer (PCET) mechanism. In the gas phase, this PCET mechanism leads to ground state recovery on a sub-ps time scale.[13–16] The capacity of DNA to efficiently dissipate the energy attained by absorption of UV radiation[1,17] is critical to reduce the damage of the genetic code,[18] further motivating the study of the CT and PCET processes in GC base pairs, both in isolation[14,15,19–24] and within DNA.[16,25–27] In a very interesting study, Röttger et al,[23] succeeded in enforcing the formation of a WC pair of GC in chloroform by using derivatives of G and C bearing very bulky substituents on the sugar, and their time-resolved spectral analysis provides very useful reference data for the study of CT process in solution in a relatively small molecular system.

[a] Dr. J. A. Green, Dr. R. Improta
Istituto di Biostrutture e Bioimmagini-CNR, Via De Amicis 95, I-80145 Napoli
E-mail: james.green@ibb.cnr.it
robimp@unina.it
roberto.improta@cnr.it
[b] Dr. S. Gómez, Prof. G. Worth
Department of Chemistry, University College London, 20 Gordon Street, London WC1H 0AJ, United Kingdom
[c] Dr. S. Gómez
Departamento de Química Física, University of Salamanca, Salamanca 37008, Spain
[d] Dr. F. Santoro
Istituto di Chimica die Composti Organometallici (ICCOM-CNR), Area della Ricerca del CNR, Via Moruzzi 1, I-56124 Pisa
E-mail: fabrizio.santoro@iccom.cnr.it

Supporting information for this article is available on the WWW under https://doi.org/10.1002/chem.202201731

At the state-of-the art, fully QD simulations still represent an open challenge, especially if the dynamical response of the solvent to the ongoing nonadiabatic transition needs to be addressed.[28] We here make a first step, focusing in the ultrafast (~100 fs) time-scale on the population of the G→C CT state, without considering the subsequent PT process. This time-regime is still challenging but more affordable, in particular if we assume that the nuclear degrees of freedom of the solvent remain frozen in the configuration they have when the photo-excitation takes place, the so-called "static disorder" limit.[29–33] However, also in this ultrafast time-scale several chemical physical effects, related both to bulk solvation and 'direct' solute-solvent interactions, can play a role in the population of a CT state, a reaction that leads to a substantial rearrangement of the solute electron density. In order to get a picture as complete as possible about such effects, as well as on the related methodological issues, we compare four different solvation models, two explicit ones and two implicit ones. For explicit models the "static-disorder" limit can be implemented by extracting a representative number of snapshots (in the specific case here, 100) from a molecular dynamics (MD) simulation of GC in the ground state in chloroform,[24] and performing different QD simulations for each of them. In these QD simulations, the solvent molecules are treated as frozen and described either at the molecular mechanical (MM) level or by treating the first solvation shell at the full quantum mechanical (QM) level. On the same ultrafast time-scale it is also possible to use implicit solvent models in their non-equilibrium implementation, where one assumes that only the fast, electronic part of the polarization is equilibrated with the excited states, while the slow nuclear part is still in equilibrium with the ground state.[28] Here we adopt the polarizable continuum model in its linear response formalism (LR-PCM),[34] and its first-order corrected (cLR) implementation.[35] A schematic representation of an implicit and explicit solvent model that we use for GC in this work is shown in Figure 1.

For the QD simulations, we exploit the recently developed fragment diabatization parametrization of a linear vibronic coupling (FrD-LVC) model[36] from time-dependent density functional theory (TD-DFT) calculations. On the time-scale of interest of this study, the system is rigid enough to be amenable to a description in terms of low-order Taylor-expansion model Hamiltonians, for which nonadiabatic QD simulations are particularly effective, as shown by our recent study of GC and AT photoactivated dynamics in the gas phase.[36,37] We also exploit advances in the multiconfiguration time-dependent Hartree (MCTDH) method[38,39] to carry out these high dimensional QD simulations, namely its extension to multilayer (ML) formalism,[40,41] and its implementation within the Quantics package.[42,43]

Our study shows that the G→C CT state is quite effectively populated in chloroform. Depending on the adopted solvation model and the electronic state initially excited, between 10–60% of the bright excited state population is transferred to G→C CT after 50 fs. However, the population transfer is less substantial and slower than that found in the gas phase (60~90%).[36] Therefore, a key result of the present work is that we observe that the formation of a CT state is disfavoured by an increase in the polarity of the embedding medium. Based on this observation, we can assess the different chemical-physical effects modulating the ultrafast population of CT states and get interesting insights on the related methodological issues. In particular, we show that a simple analysis of the solute/solvent electrostatic interactions on the energy of the CT state can provide a rather reliable indication of its possible population, and we can make general observations on the behavior of assemblies with closely positioned chromophores.

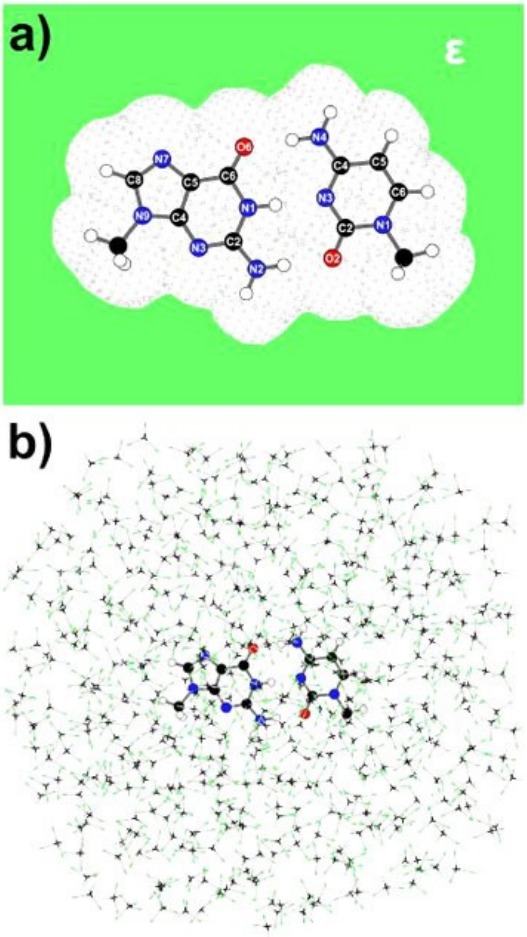

Figure 1. a) Schematic drawing and atom numbering of the 9-methylGuanine/1-methylCytosine dimer, in Watson Crick hydrogen bonding arrangement. The PCM cavity is also schematically depicted b) Schematic description of a snapshot extracted from our MD simulations with explicit chloroform molecules

Methods

FrD-LVC

The approach in this work is to use a fragment based diabatisation (FrD) for multi-chromophore complexes (MCs) to parameterise a linear vibronic coupling (LVC) model. It has been introduced in Ref. [36], and a description of the underlying

theory can be found also in Refs. [44] and [45]. It is therefore only briefly sketched below and in the Supporting Information (SI), Sections S1.1 and S1.2.

The LVC Hamiltonian for a coupled set of diabatic electronic states $|\mathbf{d}\rangle = (|d_1\rangle, |d_2\rangle, \ldots, |d_M\rangle)$ may be written as

$$H = \sum_i (K + V_{ii}^{\mathrm{d}}(\mathbf{Q})|d_i\rangle\langle d_i|) + \sum_{i,j>i} V_{ij}^{\mathrm{d}}(\mathbf{Q})(|d_i\rangle\langle d_j| + |d_j\rangle\langle d_i|), \quad (1)$$

where $\{Q_1, Q_2 \cdot\cdot, Q_N\}$ are the dimensionless normal mode coordinates, defined on the ground electronic state S_0, with conjugate momenta **P**. The kinetic K and potential V terms of the Hamiltonian are defined as

$$K = \frac{1}{2}\mathbf{P}^T\Omega\mathbf{P} \quad (2)$$

$$V_{ii}^{\mathrm{d}}(\mathbf{Q}) = E_{ii}^{\mathrm{d}}(\mathbf{Q}_0) + \lambda_{ii}^T\mathbf{Q} + \frac{1}{2}\mathbf{Q}^T\Omega\mathbf{Q} \quad (3)$$

$$V_{ij}^{\mathrm{d}}(\mathbf{Q}) = E_{ij}^{\mathrm{d}}(\mathbf{Q}_0) + \lambda_{ij}^T\mathbf{Q}, \quad (4)$$

with Ω the diagonal matrix of normal mode frequencies ω_α, λ_{ij} the vector of linear coupling constants between states i and j, $E_{ii}^{\mathrm{d}}(\mathbf{Q}_0)$ the diabatic energy of state i at the reference geometry ($\mathbf{Q}_0$, typically a ground state equilibrium geometry, see SI Section S1.2 for further details), and $E_{ij}^{\mathrm{d}}(\mathbf{Q}_0)$ an electronic coupling constant between diabatic states i and j at the reference geometry.

Treating the slow degrees of freedom

In this study we shall take solvent effects into account by integrating different models. First, the FrD-LVC procedure described in the previous section will be applied to the GC in chloroform at the PCM/TD-DFT level. In this way, we shall include the 'average' bulk solvent effect on the excited state energies and the vibrational degrees of freedom of the GC pair. Henceforth, this base level FrD-LVC model will be referred to as the PCM FrD-LVC model. In 'standard' PCM-TDDFT calculations, solvent effects are included by resorting to a linear response (LR) approach, where the response of the solvent dynamic polarization to the excitation is computed from the transition density,[35,46,47] discarding the contribution due to the variation of the electron density associated with the electronic transition.[46,48] As a consequence, it has been shown that LR-PCM is ill-suited to describe electronic transitions involving a large change of the electron density.[46,48] We thus also utilised corrected LR (cLR) calculations which include a first order correction to the energy of each excited state based on its relaxed density matrix.[35] In the following the results obtained with this approach will be labeled as cLR-PCM.

However, implicit 'mean field' approaches such as PCM or cLR-PCM cannot include the effect of different solvent configurations. These different solvent configurations can result in different excited state dynamics, which cannot be described by a single dynamics on average potentials due to the non-linear dependence of the population yield on the Hamiltonian parameters.[29,33,49] In order to take this effect into account, we will exploit explicit solvation models.

Whilst full QD calculations of mutually evolving explicit solute + solvent systems are still at the moment out of reach, we limit ourselves to the so-called "static-disorder" limit.[29] In this limit, due to their very different characteristic times, the fast intramolecular vibrations of the two nucleobases can be separated from the slow inter-molecular motions, which rule both the mutual arrangements of the two nucleobases and of the solvent around them. In practice, while all the solute + solvent degrees of freedom (DoFs) are active before the photoexcitation (and are sampled by a classical MD on the ground-state), it is assumed that only the fast DoFs move appreciably during the photoexcited dynamics on the investigated timescale (~100 fs). Although the slow DoFs are considered frozen on this ultrafast time scale, their instantaneous configuration affects the fast DoFs dynamics. This effect is introduced by computing different FrD-LVC models specific for each configuration of the slow DoFs. This separation of motions is at the basis of recent mixed quantum classical approaches we have proposed and successfully applied to the simulation of the steady-state spectra[49,50] and photodynamical processes of systems in explicit environments.[29,49]

In practice, different solvent configurations will be extracted from molecular dynamics (MD) simulations, and used with a single-point diabatisation to update the diabatic energies and constant coupling terms (i.e. $E_{ii}^{\mathrm{d}}(\mathbf{Q}_0)$ and $E_{ij}^{\mathrm{d}}(\mathbf{Q}_0)$) from the base-level PCM FrD-LVC model. In doing this we make the further assumption that the change in diabatic energies and constant coupling terms is larger and more important to the dynamics of the fast Dofs than the change in λ_{ij} terms for each snapshot, i.e. that the first order terms change slower than the zero order terms in the Taylor expansion of the potential energy surface. In principle, the coordinate dependent diagonal and off-diagonal terms λ_{ij} should also be updated, however this would require an additional $2 \times N$ QM calculations, and would be too computationally costly. This approximation also implicitly assumes that the intra-molecular equilibrium geometry of G and C does not vary with the configuration of the slow DoFs. This same approach was applied and its validity tested for a perylene diimide dimer in water/acetonitrile solution in Ref. [33]. For what concerns the relative motion of the two nucleobases, in the following we consider two models in which during the ground-state MD they are either held in a rigid arrangement or they are free to move, to separately investigate the solvent and nucleobase slow DoFs. We also consider polarization effects of the inner solvent shell, so that in summary, three models will be considered:

1. $\mathrm{Frz_{GC}}$ $\mathrm{MM_{chl}}$: Snapshots will be extracted from a MD simulation in which the solute (GC) is held in a fixed position, i.e. frozen ('Frz'), and only the solvent (chloroform, 'chl') is in motion. Then, in the re-parameterisation of the FrD-LVC model, the solvent will be treated as point charges,

also known as a molecular mechanics (MM) electrostatic embedding.

2. Frz_{GC} QM_{chl}: The same snapshots as the Frz_{GC} MM_{chl} calculations will be used, however in the re-parameterisation of the FrD-LVC model an inner solvent shell will be treated at the quantum mechanics (QM) level, with the outer solvent shell treated as point charges.
3. Mov_{GC} MM_{chl}: Snapshots will be extracted from a MD simulation in which GC, as well as the solvent, is allowed to move ('Mov'). In this way we will include the effect of the relative motion of the two bases on the Hamiltonian parameters (for further details, see Section S1.2 in the SI).

Computational Details

Electronic structure calculations have been performed with DFT for the ground state and TD-DFT for the excited states using the Gaussian 16 program.[51] We adopted the CAM–B3LYP[52] range-separated functional and the computationally convenient 6–31G(d) basis set, previously used for the study of the quantum dynamics of the GC pair in the gas phase,[36] and vibrational spectra of GC in chloroform.[53] The solvent effect of chloroform is included for the geometry optimisations and the base level FrD-LVC model by means of the polarizable continuum model (PCM).[34] All the PCM and cLR-PCM calculations have been performed at the non-equilibrium level. Within continuum approaches, such as PCM, the simplest and most commonly used approach to treat dynamical solvation effects requires the definition of two limiting time-regimes. The first, non equilibrium limit is ruled by the optical dielectric constant (for chloroform ~2) and only fast polarization (related to the electronic degrees of freedom of the solvent) is in equilibrium with the new solute electron density. Full equilibration of solvent degrees of freedom (e.g. the re-orientation of the solvation shells) requires a longer time (a few ps, for chloroform ~4 ps[54]), which falls well outside the time window of interest of this paper.

As a molecular model, we use 9-methylguanine and 1-methylcytosine to represent GC in a Watson Crick conformation. The diabatic electronic states included in the models are the two lowest bright states on each base, namely $G(L_a)$, $G(L_b)$, $C(\pi\pi^*1)$ and $C(\pi\pi^*2)$, as well as the most-stable CT state, i.e. the G→C(CT) state, defined as the one electron transition from the HOMO of G to the LUMO of C (hereafter simply GC-CT). In order to obtain these diabatic states, reference local excitations and molecular orbitals were computed on each nucleobase, including the electrostatic effect of the other nucleobase by the set of the charges from the electrostatic potential in ground electronic state (defined with the restrained electrostatic potential, RESP, model).[55] Further technical details of the electronic structure setup used for the diabatisation calculations are given in the SI, Section S1.3.

The MD snapshots were extracted every 20 ps from the simulations conducted in Ref. [24], in which GC was either kept frozen and the chloroform solvent was moving, or both GC and solvent were in motion. The GC pair in these MD simulations contained a sugar ring attached to each of the bases, in analogy with the reference experimental studies, rather than a methyl group, as is used in the LVC parameterisation. This sugar ring was kept in place, rather than substituted with a methyl group, as it only has a marginal effect on the excited state energies and characters. Indeed, the 'solvent hole' left behind if the sugar ring was substituted by the methyl group would have a slightly greater erroneous affect on the excited states, as illustrated in Section S2.1 of the SI.

QD propagations using the FrD-LVC models were performed using the ML–MCTDH method[40,41] implemented within the Quantics package.[42,43] We followed the numerical procedures used previously,[36] and further details may be found in the SI, Section S1.4. Absorption spectra of GC were calculated via the Fourier transform of the auto-correlation function produced by the QD calculations, weighted by the diabatic transition dipoles.[33,36,56] Monomeric spectra of G and C were also calculated with auto-correlation functions produced by QD propagations on LVC models parametrised by PCM(chloroform)/CAM-B3LYP/6-31G(d), in the same manner as we have previously done.[36,57] The absorption spectra include contributions from the lowest three bright states in GC ($G(L_a)$, $G(L_b)$ and $C(\pi\pi^*1)$), and are phenomenologically broadened with a Gaussian of half-width half-maximum HWHM = 0.04 eV. Further details may be found in the SI, Section S1.5.

Results

Table 1 reports the energy of the 5 lowest energy diabatic states (qualitatively similar to the starting adiabatic states, see SI Table S3) and the electronic coupling existing among them, as computed by FrD based on TD-CAM-B3LYP calculations in the gas phase and in chloroform. For the explicit solvation results, standard deviations of the energy and couplings are also reported, with histograms of their distributions shown in Section S5.1 of the SI.

Solvent has a small effect on the energy of the bright states, i.e. a weak red-shift for $G(L_a)$ and $G(L_b)$, a weak blue-shift for $C(\pi\pi^*2)$, while $C(\pi\pi^*1)$ is almost unaffected. On the contrary, in chloroform GC-CT is strongly destabilized with respect to the gas phase, especially at the PCM level, when its diabatic energy increases by 0.5 eV. As a consequence, while in the gas phase GC-CT is the most stable diabatic excited state, in chloroform its relative stability is close to that of $G(L_b)$, i.e. it has an energy 0.3 ~ 0.4 eV higher than that of $G(L_a)$ and $C(\pi\pi^*1)$. This result is likely due to the solvent effect on the frontier orbitals of G and C; for example the energy gap between the G HOMO and the C LUMO increases by ~0.15 eV going from gas phase to chloroform. The standard implementation of PCM, however, is known to underestimate the stability of excited states with significant CT character. cLR-PCM calculations, indeed, have a very modest effect on the bright states but strongly (by ~0.35 eV) stabilize GC-CT, which, though still less stable than in the gas phase, gets closer in energy to $C(\pi\pi^*1)$ and $G(L_a)$.

The average diabatic energies predicted by explicit solvation models are very close to the PCM and cLR-PCM ones for the bright states. Interestingly, the relative stability of GC-CT is intermediate between that computed at the PCM and cLR-PCM level. The solvent effect on the diabatic couplings, intra- or inter-monomer, between bright excited states is also modest. Larger shifts are instead observed for the couplings between the bright and GC-CT states, in particular at the cLR-PCM level, where $G(L_b)$ is the bright state predicted to be most strongly coupled to GC-CT, as opposed to $G(L_a)$ in the other solvation approaches. The reason for this phenomenon is related to the fact that cLR-PCM only provides a correction to the energies of the adiabatic states, without changing their character (i.e. diabatic mixing) relative to LR-PCM. The adiabatic TD-DFT states

S_3 and S_4 have mixed G(L_b) and GC-CT diabatic character and similar energies at the LR-PCM level (see Tables S2 and S3 in the SI). As GC-CT is stabilised by much more than G(L_b) with cLR-PCM, a large coupling between these diabatic states is introduced in order to produce adiabatic states with the same character as S_3 and S_4 at the LR-PCM level. This is further explained in the SI, Section S2.2.

The comparison between Frz_{GC} MM_{chl} and Mov_{GC} MM_{chl} results gives additional insights on the effect of intermolecular vibrational motions. Their inclusion by MD simulation makes the relative stability of GC-CT and its coupling with bright states slightly decrease. Furthermore, as may be expected, the dispersion of CT energies increases when GC is allowed to move. Interestingly, as we show in the SI in Section S5.2, G and C are slightly closer together when they are allowed to move, than when they are held fixed. However, there is limited correlation between the distance of the bases and CT energy. Instead, as we reveal later on, the surrounding electrostatic environment plays a much greater role.

Dynamics

Absorption spectra

As a first step of our study we calculated the absorption spectra, including nonadiabatic effects, to ensure that our simulations are able to reproduce experimentally observable features. Namely, the inter-monomer couplings triggered by the formation of the HB GC dimer are mirrored by the subtle but visible changes in its absorption spectrum with respect to that obtained from the sum of G and C absorption spectra (G + C) in chloroform, as reported experimentally.[19] In our calculation of the absorption spectrum, we do not consider a direct excitation to the second bright excited state of Cytosine, and this approximation obviously affects the accuracy of the lineshape of the high energy part of the spectrum. Nonetheless, as discussed in the SI Section S4.1 and shown in Figure 2, our calculations nicely reproduce the difference between GC and G + C absorption spectra. Indeed the former spectrum is more intense and less resolved close to the maximum of the absorption band, whereas the absorption in the red wing is slightly reduced. Inclusion of explicit solute/solvent interactions, as could be expected, improves the agreement with the

Table 1. Diabatic energies ($E^d_{ii}(Q_0)$) and constant electronic couplings ($E^d_{ij}(Q_0)$) in eV of bright ππ* and CT states of GC in C_s symmetry from all solvent models considered in this study. Explicit solvation results are averaged over all snapshots, the couplings being the average of absolute values, and standard deviations in parentheses. Parametrized using CAM-B3LYP/6-31G(d).

State *i*	State *j* G(L_a)	G(L_b)	C($\pi\pi$*1)	C($\pi\pi$*2)	GC-CT
	Gas				
G(L_a)	5.311				
G(L_b)	0.083	5.682			
C($\pi\pi$*1)	−0.011	0.020	5.286		
C($\pi\pi$*2)	0.061	−0.019	0.087	5.936	
GC-CT	0.072	−0.021	0.030	−0.031	5.138
	PCM				
G(L_a)	5.199				
G(L_b)	0.083	5.639			
C($\pi\pi$*1)	−0.015	0.018	5.256		
C($\pi\pi$*2)	0.053	−0.010	0.114	6.021	
GC-CT	0.072	−0.014	0.037	−0.025	5.637
	cLR-PCM				
G(L_a)	5.223				
G(L_b)	0.088	5.556			
C($\pi\pi$*1)	−0.021	0.030	5.288		
C($\pi\pi$*2)	0.050	−0.007	0.108	6.015	
GC-CT	0.040	0.145	0.006	−0.029	5.274
	Frz_{GC} MM_{chl}				
G(L_a)	5.273 (0.026)				
G(L_b)	0.063 (0.005)	5.645 (0.025)			
C($\pi\pi$*1)	0.003 (0.002)	0.025 (0.001)	5.284 (0.038)		
C($\pi\pi$*2)	0.055 (0.005)	0.026 (0.004)	0.075 (0.007)	6.136 (0.056)	
GC-CT	0.056 (0.002)	0.026 (0.003)	0.029 (0.001)	0.021 (0.008)	5.453 (0.205)
	Frz_{GC} QM_{chl}				
G(L_a)	5.208 (0.035)				
G(L_b)	0.073 (0.021)	5.539 (0.038)			
C($\pi\pi$*1)	0.005 (0.003)	0.021 (0.001)	5.250 (0.055)		
C($\pi\pi$*2)	0.052 (0.004)	0.021 (0.005)	0.105 (0.014)	6.047 (0.068)	
GC-CT	0.058 (0.007)	0.032 (0.005)	0.030 (0.003)	0.018 (0.008)	5.553 (0.207)
	Mov_{GC} MM_{chl}				
G(L_a)	5.241 (0.040)				
G(L_b)	0.049 (0.010)	5.736 (0.045)			
C($\pi\pi$*1)	0.016 (0.004)	0.023 (0.002)	5.209 (0.054)		
C($\pi\pi$*2)	0.050 (0.009)	0.012 (0.006)	0.061 (0.012)	6.048 (0.075)	
GC-CT	0.054 (0.020)	0.013 (0.009)	0.027 (0.014)	0.018 (0.013)	5.576 (0.291)

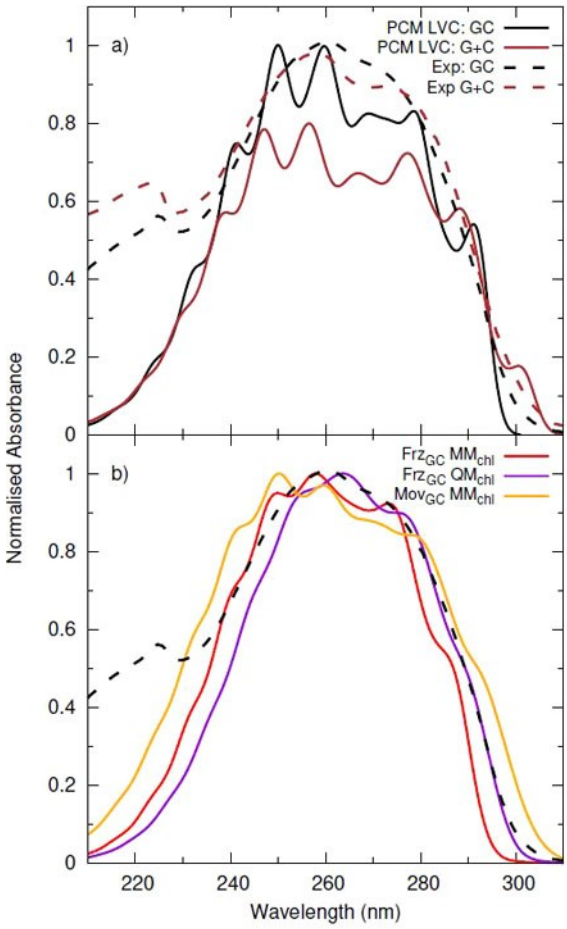

Figure 2. a) Absorption spectra of GC, and the sum of monomer G and C (G + C) spectra either calculated from PCM FrD-LVC models (solid lines), or from experimental results in chloroform (dashed lines).[19] b) Spectra from explicit solvation FrD-LVC models, averaged over the 100 snapshots dynamics. Intensity of the most intense peak of the GC spectra normalised to 1, with the G + C spectra normalised with the same value. FrD-LVC spectra shifted by −0.65 eV.

experimental spectra, decreasing the resolution of the computed spectra and increasing its broadness.The spectral lineshapes in Figure 2 show some peaks, due to vibronic transitions. They are more evident in the PCM computations and are stronglly smoothed out in explicit solvent due to solvent fluctuations. Such a vibronic structure is almost completely washed out in the experiment, indicating that our approach still underestimates the solvent inhomogeneous broadening.

Excitation to G(L$_a$)

As discussed in detail in the SI Section S2 and further below, the different diabatic states are slightly mixed in the Franck-Condon (FC) region. It is clear that the four lowest adiabatic states derive from a combination of G(L$_a$), G(L$_b$) and C($\pi\pi$*1) states, together with GC-CT. In the following, we shall discuss the photoactivated dynamics of GC following an excitation to each of these low energy bright states, focusing our discussion in the population of GC-CT and starting from G(L$_a$).

Figure 3 shows that inclusion of solvent effect leads to a strong decrease of the G(L$_a$)→GC-CT population transfer. In the gas phase after ~50 fs 90% of the photoexcited population is on GC-CT. This value decreases to ~50% at the Frz$_{GC}$ MM$_{chl}$ level; ~30% at the Mov$_{GC}$ MM$_{chl}$, Frz$_{GC}$ QM$_{chl}$, and cLR-PCM levels; and it is only ~10% according to PCM calculations. The population of GC-CT then increases at later times according to all the models, but, even after 250 fs it never reaches the level (>90%) predicted in the gas phase. The solvent CT populations also demonstrate some small oscillatory features with a period of ~20 fs, most noticeable in the PCM model and predominantly averaged out in the explicit solvation models. These are essentially due to vibronic coherences of the ring stretching and NH2 bending motions of G and C, with typical vibrational frequencies of ~1600 cm^{-1}. This is further discussed in Section S3.2 of the SI.

As shown in Figure 4, the 100 QD simulations starting from structures extracted from the MD simulations show that the static disorder has a huge effect on the population of GC-CT. Interestingly, the average values are not representative of the trends of the different simulations. Indeed we observe that for a significant portion of the structures we have ~80% of the population on GC-CT after 50 fs, whereas for several others the transfer is very small (<20%) (see also Table 2). In other words, we are in the presence of an 'on/off' picture where, depending on the initial arrangement of the solvent molecules, the transfer is either almost quantitative or it does not happen at all. In the following subsections, we shall discuss what the chemical/physical effects are that account for the significant dependence of the population transfer to GC-CT on the initial solvent configuration.

In terms of the different explicit solvation approaches, the averaged populations of the GC-CT state follow the trend of GC-CT energies calculated by each method. Frz$_{GC}$ MM$_{chl}$ predicts the greatest population and also most stable GC-CT state, with

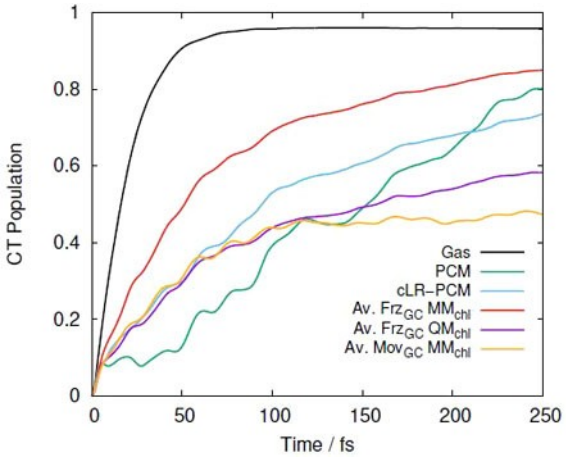

Figure 3. GC-CT population after initial excitation to G(L$_a$) with different solvation approaches: gas phase, LR-PCM, cLR-PCM, and average over 100 Frz$_{GC}$ MM$_{chl}$, Frz$_{GC}$ QM$_{chl}$, and Mov$_{GC}$ MM$_{chl}$ snapshots.

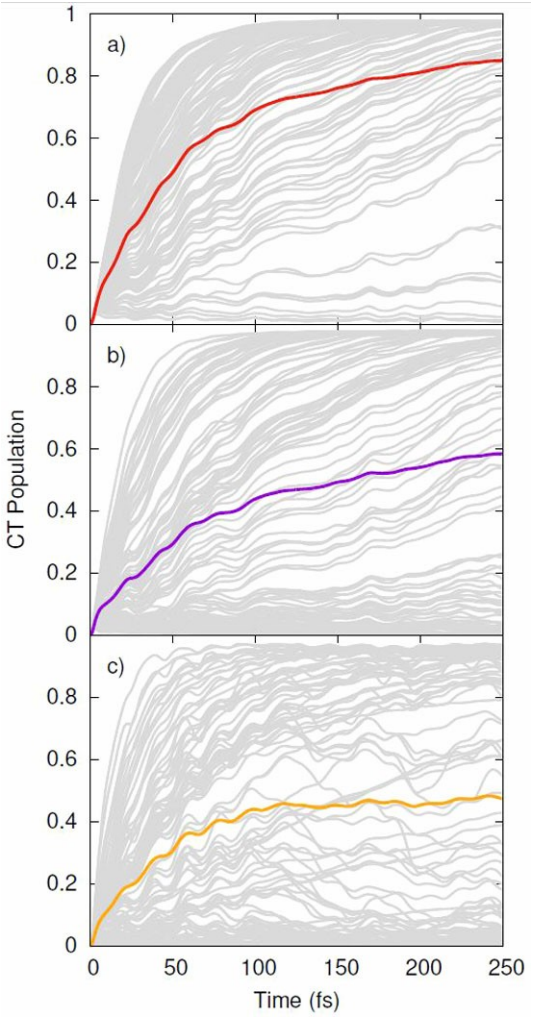

Figure 4. GC-CT population after initial excitation to G(L_a) for a) Frz_{GC} MM_{chl} snapshots and their average b) Frz_{GC} QM_{chl} snapshots and their average and c) Mov_{GC} MM_{chl} snapshots and their average.

smaller population predicted by Frz_{GC} QM_{chl} and then Mov_{GC} MM_{chl}. In the latter case, the relative stability of GC-CT slightly decreases, as it is not only the solvent that is causing the destabilisationof the GC-CT state, but also the motion of the bases. This result gives an account of the smaller transfer to GC-CT and explains the greater dispersion of energies and couplings, as well as greater dispersion of the individual snapshot dynamics and more oscillation in the GC-CT populations, as shown in Figure 4. Further analysis of the relation between couplings and dimer structure is reported in SI Section S5.2.

We end this section by noting that single QD propagations performed using the averaged explicit solvent parameters shown in Table 1 produce slightly different results to the average over 100 simulations as shown in Figures S7–S12 in the SI, in particular for the Mov_{GC} MM_{chl} and Frz_{GC} QM_{chl} approaches. This is similar to the non-linear behaviour of the averaged populations with respect to the Hamiltonian parameters some of us have observed for other systems previously.[29,33,49]

Excitation to G(L_b)

As shown in Figure 5, after excitation to G(L_b) a significant part of the photoexcited population is transferred to GC-CT, but this process is less effective than in the gas phase, according to all the solvation approaches except cLR-PCM. In this latter case, the very large G(L_b):GC-CT coupling leads to a very fast and substantial population transfer: after less than 25 fs 60% of the photoexcited population is on GC-CT. For the same reason, the cLR-PCM method is the only one predicting a substantial direct G(L_b)→GC-CT population transfer, with the population of G(L_a) always ≤0.20. The other methods indicate instead that most of the population follows a path G(L_b)→G(L_a)→GC-CT, with G(L_a) being the most populated state at t = 50 fs as shown in the Figures collected in Section S3 of the SI. However, also at the cLR-PCM level, the 'final' population of GC-CT after 250 fs is smaller than in the gas phase. The transfer rates predicted by the other methods are, overall, quite similar to those obtained for G(L_a). Furthermore, the comparison between the average of the QD simulations by using an explicit solvation model and the different snapshots shown in Figure S13 in the SI shows a similar 'on/off' behaviour for the population transfer to GC-CT.

Table 2. Percentage of simulations with GC-CT population after 250 fs propagation of less than 0.2, greater than 0.8, or in between, for all the explicit solvation snapshots after excitation on G(L_a), G(L_b) and C($\pi\pi^*1$).

Init. State	CT pop < 0.2	0.2 < CT pop < 0.8	CT pop > 0.8
	Frz_{GC} MM_{chl}		
G(L_a)	7%	14%	79%
G(L_b)	9%	10%	81%
C($\pi\pi^*1$)	7%	34%	59%
	Frz_{GC} QM_{chl}		
G(L_a)	32%	18%	50%
G(L_b)	37%.	12%	51%
C($\pi\pi^*1$)	30%	32%	38%
	Mov_{GC} MM_{chl}		
G(L_a)	42%	19%	39%
G(L_b)	45%.	15 &	40%
C($\pi\pi^*1$)	43%	29%	28%

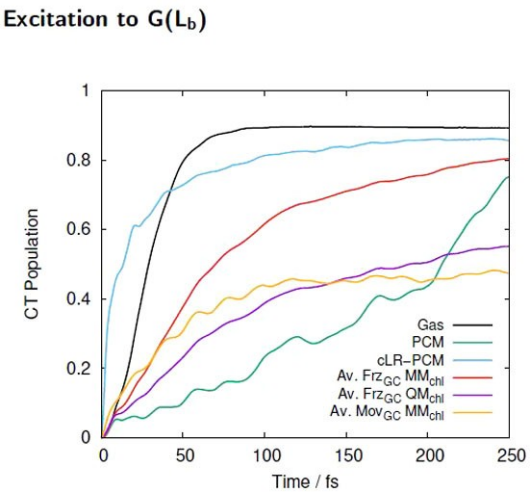

Figure 5. CT population after initial excitation to G(L_b) with different solvation approaches: gas phase, LR-PCM, cLR-PCM, and average over 100 Frz_{GC} MM_{chl}, Frz_{GC} QM_{chl}, and Mov_{GC} MM_{chl} snapshots.

*Excitation to C(ππ*1)*

In the gas phase the population transfer C($\pi\pi^*$1)→GC-CT is less complete and occurs at a slower rate than for G(L_a) and G(L_b), which as previously noted is due to smaller diabatic C($\pi\pi^*$1):GC-CT coupling than G(L_a):GC-CT.[36] In chloroform the C($\pi\pi^*$1):GC-CT coupling is also smaller than that of G(L_a):GC-CT, and the population transfer to the GC-CT state is slower and less complete, as shown in Figure 6. Independently of the solvent model, after 50 fs the population of GC-CT is $\lesssim$0.30. In particular, due to the very small electronic coupling, at the cLR-PCM level after 50 fs the GC-CT population is only ~0.05. As shown in the Figures collected in Section S3 of the SI, the rest of the population mainly remains on the C($\pi\pi^*$1) state, with some ($\lesssim$0.2) 'excitonic' transfer to the G(L_a) state. For the explicit solvation models, Figure S15 in the SI illustrates a slightly reduced 'on/off' behaviour of the individual snapshot GC-CT populations relative to the initial excitations on G, with more in the intermediate region and similar to the averaged line.

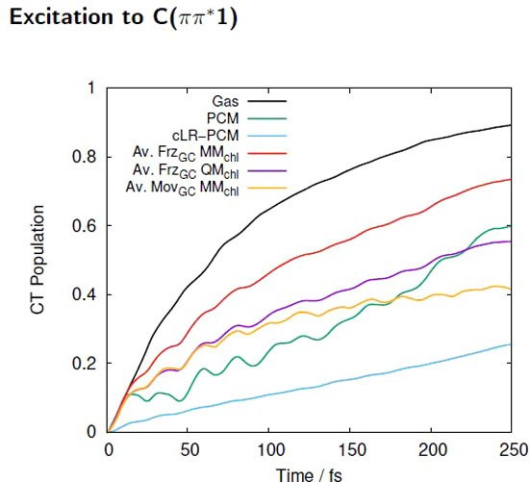

Figure 6. CT population after initial excitation to C($\pi\pi^*$1) with different solvation approaches: gas phase, LR-PCM, cLR-PCM, and average over 100 Frz_{GC} MM_{chl}, Frz_{GC} QM_{chl}, and Mov_{GC} MM_{chl} snapshots.

Dynamics initiated on the adiabatic LVC states

In the complex system we are considering, with many coupled electronic states, simulating the excitation process is not a trivial task. The most direct and precise approach would be to introduce the excitation step directly in the QD simulation, i.e. explicitly considering the coupling with the laser pump in the TD Hamiltonian. However, due to its computational cost, this approach is unaffordable for large systems, such as that which we consider in this work. In this context, the excitation of a diabatic state, beyond being convenient from the technical point of view, corresponds to a well defined impulsive limit. The pulse is so short in time to excite a doorway state corresponding to a diabatic state, but not so short to excite directly the combination of all of them. However, each of the diabatic states considered here is actually spread on more than one adiabatic state. In their experiment, Schwalb and Temps[19] adopted pulses with a FWHM in time of 200 fs, corresponding to a FWHM of ~0.02 eV in the energy. It is therefore questionable if they could excite a pure diabatic state, considering that, for example, the energies of G(L_a) and C($\pi\pi^*$1) lie approximately in this window. Therefore, due to the lack of simulations which explicitly address the excitation step, as final check of the robustness of our prediction with respect to the adopted reference states, we also considered the limiting situation in which the excitation prepares an adiabatic state and we started our simulations from the linear combination of the diabatic states that corresponds to the pure LVC adiabatic states S_1-S_4, according to the PCM calculations. The eigenvectors of these adiabatic states in terms of the diabatic states are shown in Table S4 in the SI, as well as their oscillator strengths. This approach also provides a point of comparison for any future 'on-the-fly' dynamics studies, which work in the adiabatic basis due to interfacing with electronic structure codes for the construction of the potential energy surfaces.[58]

We obtain a picture (summarized in Figure 7) very similar to that described based on LR-PCM diabatic states. In particular, we confirm the strong coupling between G(L_a) and GC-CT, which provides the main contributions to S_1 and S_3. When S_1 and S_3 are excited (the latter of which is almost dark), the majority of the population 'localizes' on GC-CT. This process is, however, far from being complete. Indeed, a significant fraction of the population remains on the bright excited states. Interestingly, after exciting S_1 and S_3 we have an almost 'constant' population (10~20%) of C($\pi\pi^*$1) for the entire propagation period, reflecting the limited excitonic transfer from G(L_a) to C($\pi\pi^*$1) or vice-versa. Analogously, simulations starting from S_2 (where C($\pi\pi^*$1) has the largest weight), provides a significant population of G(L_a), while the population

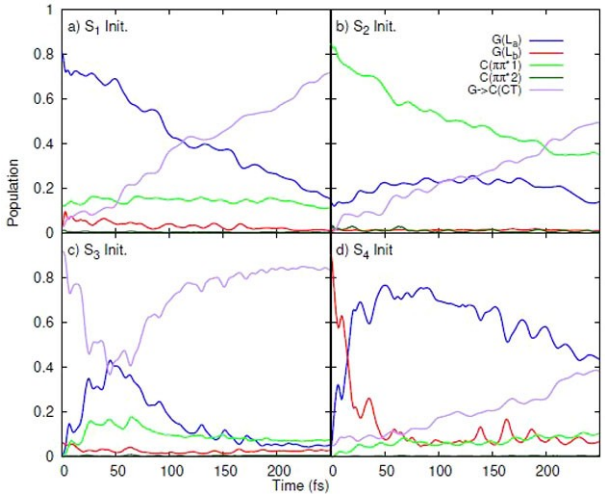

Figure 7. Diabatic populations after initial excitation to the adiabatic a) S_1, b) S_2, c) S_3 and d) S_4 states constructed as a linear combination of diabatic states, based on the LR-PCM Hamiltonian.

of GC-CT is less substantial than for S_1 and S_3. Finally, after exciting S_4, a very fast $G(L_b)\rightarrow G(L_a)$ population transfer is found, followed by partial transfer to GC-CT.

Analysis of the explicit solvent effects

Based on the outcome of our QD simulations, in this section we shall analyse what are the main chemical physical effects modulating the population of GC-CT. The decay from the bright excited state to GC-CT is particularly effective, notwithstanding GC-CT is not the most stable state in the FC region, and 0.3 ~ 0.4 eV less stable than the lowest energy bright states of G and C. This result is due to the large reorganization energy of GC-CT, almost 1 eV, making its minimum ~0.1 eV more stable than the predicted diabatic minima of $G(L_a)$ and $C(\pi\pi^*1)$ (see Table S5 in the SI).

Due to the stability of the GC-CT minimum, and its relatively large electronic coupling to the bright states when compared to the excitonic couplings between bright states, even a small population of GC-CT soon after the excitation in the FC region translates into a subsequent significant population transfer to GC-CT. On these grounds we can explain why, despite the dispersion between the different trajectories, our MD-based calculations provide an 'on-off' picture, with most of the simulations predicting a GC-CT population of either >0.8 or <0.2 by 250 fs, as shown in Table 2. This is particularly the case for the initial excitations on G, with 80–90% of the snapshots falling in these windows in each of the explicit solvation approaches. As shown in Figure 8, these populations are correlated with the GC-CT energy, and hence the gap to the bright states at t = 0 fs in the FC region. When the energy gap with the bright state is too large ($\geq$ 0.45 eV), we do not observe any significant GC-CT population. When it is $\leq$ 0.35 eV, we almost always find a quantitative population transfer to GC-CT. In the quite narrow energy window in between these two regimes, there is mainly intermediate GC-CT population. We find some exceptions to this picture for the Mov_{GC} MM_{chl} snapshots, where there is more variation in the bright to GC-CT coupling strengths. Furthermore, for initial excitation of C-($\pi\pi^*1$), our simulations suggest that when the GC-CT state is more stable than $C(\pi\pi^*1)$ the population transfer to GC-CT is smaller. This difference between the initial excitations on $G(L_a)$ and $C(\pi\pi^*1)$ could reflect the smaller coupling that C(It $\pi\pi^*1$) has with GC-CT.

In order to get additional insights on the effects ruling the relative stability of GC-CT, we have examined in greater detail the electrostatic effect of the explicit solvent, initially by taking

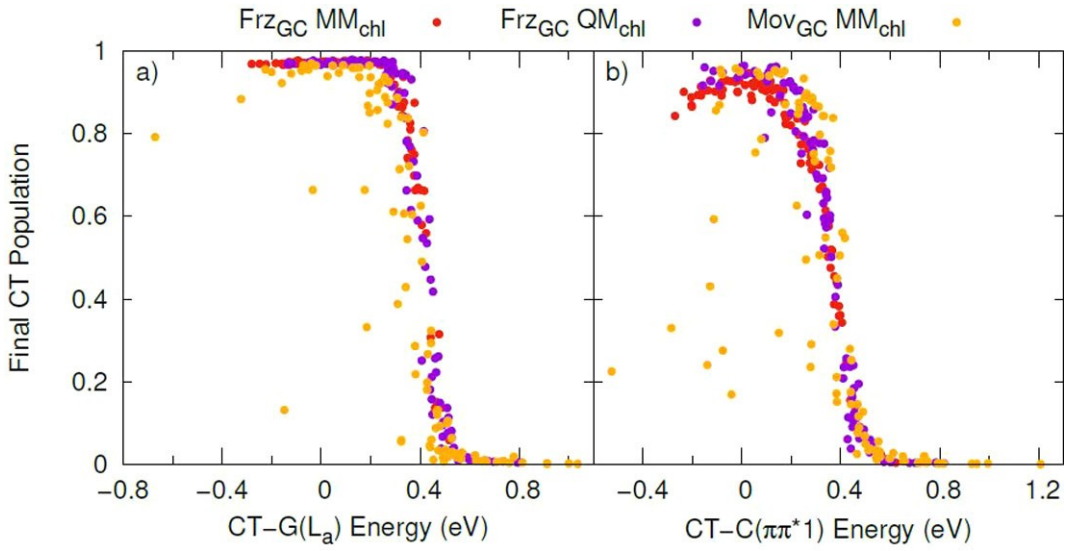

Figure 8. Correlation between the final (t = 250 fs) CT population and the initial (t = 0 fs) diabatic energy gap between the CT state and bright state excited, for excitation of a) $G(L_a)$ and b) $C(\pi\pi^*1)$ with all explicit solvation approaches.

one of the Frz_{GC} MM_{chl} snapshots as an example, and then generalising to all 100 snapshots. The snapshot we have chosen to make the example is one which has a high GC-CT energy, and hence low population following excitation on G or C. Its structure with closest surrounding explicit solvent is shown in Figure 9, and 4 hydrogen atoms of the chloroform solvent closest to G are marked. H1 and H2 are hydrogen bonded to N3 on G, and H3 and H4 are hydrogen bonded to the carbonyl oxygen of G. H4 is also quite close to the amino N of C (2.39 Å).

We tested the effect of removing these hydrogen atoms in our FrD Frz_{GC} MM_{chl} calculated diabatic energies (i.e. by setting the charge associated with these solvent hydrogen atoms to zero), with the results shown in Table 3. When all the solvent atoms are included, the GC-CT energy lies approximately 0.5 eV higher than G(L_a) and C($\pi\pi^*1$). Removing the H1 and H2 atoms stabilises GC-CT by ~0.5 eV, whilst the bright states are virtually unaffected (and similarly the couplings are also unaffected – see Table S6 in the SI), leading to GC-CT being approximately isoenergetic with G(La) and C($\pi\pi^*1$). Removal of H3 has a similar, although slightly less pronounced stabilisation of GC-CT by ~0.4 eV, whilst H4 (which also lies close to C) has virtually no effect on the GC-CT energy.

In order to generalize the analysis of the solute/solvent electrostatic interactions on the GC-CT energy, in Figure 10 we show the Frz_{GC} MM_{chl} calculated diabatic GC-CT energies, plotted versus the difference between solute-solvent Coulomb potential energy calculated for neutral GC in its ground state geometry (V^{chl}_{GC}) and G^+C^- at the same geometry ($V^{chl}_{G^+C^-}$). These Coulombic potential energies were calculated between point charges on the N_{chl} solvent atoms q_m, and point charges on the

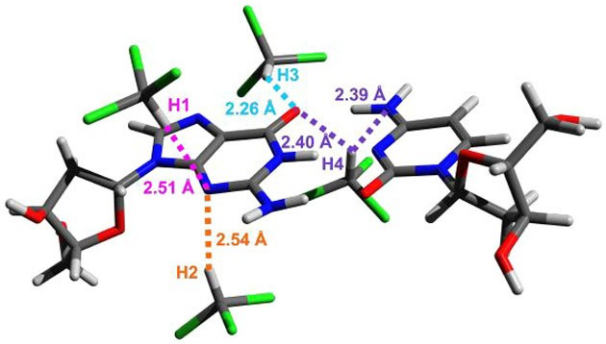

Figure 9. Closest solvent H atoms to G in an example snapshot from the Frozen MD simulation, with distances and labels. H1 and H2 are closest to G(N3), and H3 and H4 closest to G carbonyl O. H4 is also close to the amino group of C.

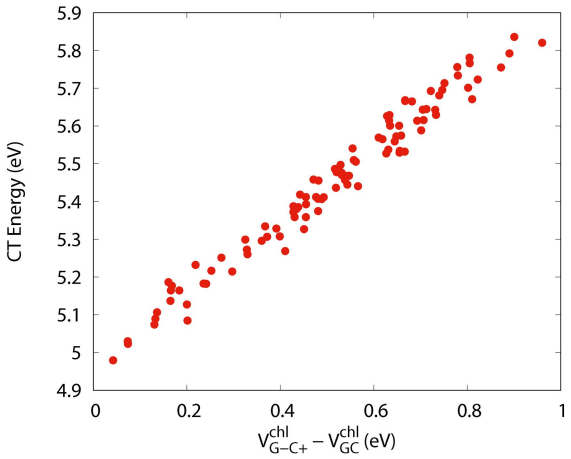

Figure 10. Diabatic Frz_{GC} MM_{chl} GC-CT energies, plotted versus the difference in solute-solvent Coloumb potential energies computed for neutral GC (V^{chl}_{GC}) and G^+C^- ($V^{chl}_{G^+C^-}$) according to eq. 5.

N_{GC} atoms of the nucleobases q_n at a distance r_{mn} at the Frz_{GC} MM_{chl} geometries (not including the sugar rings). The charges on the nucleobase atoms were obtained from RESP charges on either the neutral or ionic species

$$V^{solvent}_{solute} = \sum_{m}^{N_{chl}} \sum_{n}^{N_{GC}} \frac{q_m q_n}{r^2_{mn}}. \quad (5)$$

The Coulombic potential energy differences shown in Figure 10 are always positive, i.e. the solute/solvent interaction is more favorable for neutral GC, and this is not surprising, as the MD simulation from which the snapshots were extracted was conducted using neutral GC. Some of the potential energy differences are close to zero, however, reflecting solvent configurations that stabilize equally also the charged species, and hence yield the lowest GC-CT energies. Conversely, some solvent configurations yield GC-CT energies that are almost 1 eV less stable, and there is a linear relationship between the GC-CT energy and this Coulombic potential energy difference.

A similar analysis was also performed for the Mov_{GC} MM_{chl} snapshots in Section S5.2.3 in the SI. In this case, it is necessary to take into account not only the electrostatic effect of the solvent molecules, but also that of the bases on one another, whose arrangement is different for each snapshot. We observe also in this case a linear trend with respect to the CT energy.

Table 3. Diabatic energies ($E^d_{ii}(0)$) of bright $\pi\pi^*$ and CT states of the example Frz_{GC} MM_{chl} snapshot, computed including either all the surrounding charges associated with solvent, or with selected hydrogen atoms close to G removed (see Figure 9).

	G(L_a)	G(L_b)	C($\pi\pi^*1$)	C($\pi\pi^*2$)	GC-CT
All	5.263	5.654	5.266	6.182	5.723
H1 Removed	5.270	5.619	5.256	6.141	5.205
H2 Removed	5.253	5.623	5.253	6.143	5.274
H3 Removed	5.255	5.670	5.289	6.128	5.359
H4 Removed	5.287	5.674	5.356	6.065	5.795

Discussion

According to the QD simulations reported in the previous section, the population of GC-CT in the GC pair in chloroform is fast and effective. A significant part of the population initially excited on C($\pi\pi$*1), G(L_a), and G(L_b) decays to GC-CT, the state with the largest reorganization energy. After 250 fs, independently of the adopted solvation model, at least 50% of the population is on GC-CT. Even after 50 fs, the time window for which our approach should be fully reliable (see below), the simulations predict that the population of GC-CT is 0.3 ~ 0.4.

However, and this is one of the key results of our study, the population transfer is less complete and occurs at a slower rate than in the gas phase according to almost all the solvation models, in line with the relative destabilization of GC-CT in chloroform. At first sight, this is a surprising result. Though chloroform is not very polar, an increase of the polarity of the embedding medium is expected to stabilize a CT state, whose population involves a large increase of the electric dipole moment. On the other hand, its dipole moment is not the only property determining solvent effect on a given excited state. Solvent can change the excitation energies also by affecting the energy of the MOs involved.[46] This effect can be particularly meaningful for CT states, which involve MOs located on two different moieties. As a consequence, a rather modest solvent effect on the MOs of the bright states, which are located on the same base, can translate into a more significant one for CT states, as happens for GC.

At the standard LR-PCM level, when compared to the gas phase, GC-CT is relatively destabilized by ~0.5 eV with respect to the bright states, and it has been shown that this level of calculation can capture solvent effects on the MOs.[46,47] On the other hand, LR-PCM calculations can significantly underestimate the solvent stabilization of CT states,[35,46,48,59] whose treatment necessitates the inclusion of terms explicitly depending on the excited state density, such as cLR-PCM or SS-PCM.[35,46,48,60] In fact, at the cLR-PCM level, GC-CT is significantly stabilized but, remarkably, it is still less stable than in the gas phase. The stabilisation of the GC-CT state to a lower energy than in the gas phase instead arises due to dynamical solvation effects, i.e. the part of the solvation that takes a finite-time and depends on the movement of the solvent molecules to go from a non-equilibrium to equilibrium regime. With a continuum model, this is easily shown (see SI Table S2 and surrounding text) by the fact that at the equilibrium level (ruled by the static dielectric constant) GC-CT is, largely, the most stable excited state in the FC region.

Analogously, coherently with the timescale under investigation, within the explicit solvation models considered in this work, we have not allowed the solvation shell to move and re-orient according to the excited state density, and hence they describe the non-equilibrium regime. Interestingly, the excited state energies computed with explicit solvent models are intermediate between those predicted by PCM and cLR-PCM. The explicit solvation approaches also provide insights on the role played by static disorder effects, i.e. those related to the particular arrangement of the solvent molecules when GC is excited. In fact, though the average picture provided by the 100 QD simulations is fairly similar (though not the same) to that of the single QD result with LR-PCM parameters, the predictions of the single simulations exhibit dramatic differences, with many simulations indicating a quantitative transfer to GC-CT and several for which no transfer occurs. As discussed in the previous section, our analysis indicates that the energy of the GC-CT state is sensitive to the HB arrangement of the chloroform molecules.

Moreover, we have shown that the energy gap between GC-CT and the bright states linearly depends on the difference between the solute/solvent electrostatic interaction energy in the ground and in the CT state. Since the bright states are less sensitive to the particular arrangement of the solvent molecules, the CT population is essentially ruled by the CT energy at different snapshots. This can be easily estimated by a simple electrostatic calculation, without resorting to expensive QD simulation. In other words, once the trends shown in Figure 8 and Figure 10 have been established, even based on a relatively small number of QD propagations, it is possible to 'predict' if the transfer to GC-CT occurs, only by processing the MD simulations. In principle, this procedure could be easily extended to the study of other MCs, to rationalize and/or predict the extent of CT population, at a reasonable computational cost, provided that these systems are in strong CT driving force regime. More precisely, we can define this regime as the case when the bright-CT electronic coupling is similar to or greater than the excitonic coupling, and the CT reorganisation energy is greater than that of the bright state. To confirm this hypothesis, we plan to perform further tests in this direction in the near future on different MCs. We note that more sophisticated treatments of the electrostatic effects are possible,[61] and recent work has demonstrated their ability to calculate CT energies for a perylene diimide system.[62]

Despite its focus on the ultrafast part of the photoactivated dynamics and the lack of the PT reactive channel, our simulations provide useful indications for the interpretation of the time resolved experiments on GC in chloroform.[23] Indeed, the population of GC-CT is a necessary step for the occurrence of PCET.[14] In this respect, our calculations confirm that in chloroform the population of GC-CT is effective and very fast, in line with the very fast appearance of transient absorption spectra spectra typical for the $G^{\bullet+}$ cation or G–H$^{\bullet}$ radicals.[23] Assigning this transient spectra to the G–H$^{\bullet}$ radical, it has been proposed that within 40 fs $\geq$60% of the photoexcited state population has undergone a PT reaction.[23] Our simulations cast some doubts about this conclusion, because on that time scale the population of GC-CT is too small. It is possible that the high similarity between the absorption spectra of $G^{\bullet+}$ and G–H$^{\bullet}$,[63,64] especially when bonded to C,[65] makes it difficult to discriminate between these two species.

Our calculations also give account of the smaller yield for the PCET reaction observed when exciting at 290 nm[15,23] compared to exciting at 260 nm.[23] In fact, on the red tail of the absorption band the relative contribution of C($\pi\pi$*1) is larger and its population, according to our QD simulation, is trans-

ferred to GC-CT less effectively than an initial population on G, prevalent for an excitation at 260 nm.

Conclusions

In this study, we simulate, at a full QD level, the ultrafast photoactivated dynamics of GC pairs in chloroform solution, exploiting our recently developed FrD-LVC model, the ML–MCTDH propagation method, and comparing several different solvation models, both explicit and implicit. We predict that, on average, ~50% of the photoexcited population decays to the G→C CT within 100 fs of the excitation. The population transfer to GC-CT is larger and faster when exciting one of the two excited states localized on G, and, therefore, will be larger closer to the maximum of the absorption band and smaller in the red-tail. Our predictions are thus consistent with the available experimental results in chloroform,[23] which shows that the signature of PCET processes (triggered by GC-CT population) is less effective when exciting in the red-wing of the absorption tail.[15,23]

A quite remarkable result we get is that the population of GC-CT is significantly less effective in chloroform than in the gas phase.[36] Although a strong increase of the dipole moment is associated to the CT transition, in the ultrafast time scale when the solvent molecules have no time to move, GC-CT is relatively more stable in the gas phase, where it is the lowest energy S_1 excited state,[36] rather than S_3 or S_4 in chloroform. This result is explained by the effect that bulk solvation has on the energy of the frontier orbitals of the GC pair. Full equilibration of solvent degrees of freedom, which would strongly stabilize GC-CT, requires a finite time of a few ps,[54] longer than that here investigated. However, even if GC-CT is not the most stable excited state in the FC region, it is populated within 50 fs. Indeed, GC-CT has a large coupling to the bright states (especially those of G), and it is the state with the largest reorganization energy, i.e. its minimum is very stable. Indeed, the reorganization energy of the excited states localized on the monomers is decreased by the localization of HOMO and LUMO on the same ring. As a consequence, any geometry distortion driven by the excitation in a given bond is limited by 'intrinsic' restraints induced by the other bonds. In the minimum of GC-CT, the structure of G and C can evolve 'independently' to that of G^+ and C^-, strongly stabilizing the resulting minimum.

Our simulations using explicit solvation models show that static disorder effects, i.e. the fact solvent can be in many different configurations when photoexcitation takes place, strongly modulate the CT processes. By using the same electronic and solvation models, we observe that the population of GC-CT can vary from ~1 to ~0, depending on the instantaneous solvent configuration. Interestingly, analysis of these simulations point out the possibility to make a simple estimation of the extent of the transfer to GC-CT. Indeed, we have shown that GC-CT can be predicted to be populated based only on its energy in the FC region. There is a well defined window of the energy gap of the GC-CT state with respect to the bright ones, for which the CT can occur. Furthermore, we have also shown that a simple correlation exists between the energy of GC-CT and the solute/solvent electrostatic interactions.

From the methodological point of view we have shown that the "static disorder approach" can be nowadays routinely applied to confidently study the solvent effect on ultrafast (50~100 fs) nonadiabatic quantum dynamics also for systems as complex as the GC basepair in condensed phase. This achievement is thanks to the effectiveness of LVC parameterizations and ML–MCTDH propagations. It should be noted, however, that as we only update the zero-order elements of our Hamiltonian with the static disorder effects, we do not consider that different configurations could give rise to different excited state reorganisation energies, which could perturb the linear relationship we observe between solute/solvent electrostatics and CT energy. However, such an effect will also surely be correlated with longer time dynamical solvation effects when the motion of the solvent is coupled with the solute vibronic wavepacket. The design of reliable and effective approaches for this task is an open challenge,[28] although some of us[29] and others[30,32,66,67] have made progress in this direction. Although all the adopted solvation models provide the same qualitative indications, i.e. that the ultrafast population transfer to GC-CT in chloroform is smaller than in the gas phase, significant quantitative differences are observed. On average, PCM calculations significantly disfavour the population of GC-CT, when compared to the average predictions obtained by explicit simulations. This result confirms that LR-PCM is not suitable to describe excited electronic states involving a large change in the electron density, such as those with significant CT character.[46–48,68] It is clear that explicit solvation models are more suitable to describe disorder effects, and, eventually, the dynamical coupling between solute and solvent degrees of freedom. In this case, our study further highlights the importance of basing any conclusion on meaningful statistical sampling of the trajectories. Indeed, the 'average' dynamical picture provided by our simulation can be very different with respect to that provided by a single trajectory. The differences between Frz_{GC} QM_{chl} and Frz_{GC} MM_{chl} predictions highlight that the treatment of mutual solute/solvent polarization can also be important, particularly when one considers strongly hydrogen bonding/more polar solvents and close lying electronic states. Addressing these effects, for instance with polarizable force fields, in combination with nonadiabatic dynamics gives rise to a number of open questions discussed for instance in Ref. [69]. In future studies, we shall further explore the potentialities of mixed QM/MM approaches and, also, mixed implicit/explicit solvation models to describe the photoactivated dynamics in solution.

It should be mentioned that alternative vibronic models with treatment of solvent in a system-bath picture have been proposed in the literature. They are based on the definition of spectral densities obtained from a Fourier transform of the fluctuations of the energy gap between the adiabatic excited and the ground state during a long MD run. This approach is very powerful for weakly-coupled chromophores or when the electronic character of the target excited state does not change

during the MD sampling. This is not the case for strongly coupled systems like GC. For these cases, such a procedure should be generalized by combining it with a suitable diabatization technique. To the best of our knowledge this has been done only in one study, dealing with the coupling of only two excited states, one bright and the other dark.[70] In the future it could be interesting to test this approach with more general diabatization schemes, like the maximum-overlap one adopted here.

Our analysis also provides useful information not only for the interpretation of the experimental studies on GC, but also some general insights on the effect of the solvent on the population of 'dark' CT states from the bright, spectroscopic states. This is a key step in many processes of biological and technological interest, such as in light harvesting complexes where the electrostatic effects of surrounding protein could influence the energy and directionality of CT states,[6] or in organic photovoltaic devices, where the offset between photo-excitation and CT energy at the donor:acceptor interface can play a key role in device efficiency.[71] Within a regime in which a CT state has an electronic coupling to a bright state similar to or greater than an excitonic coupling, and large reorganisation energy, we have found that the population of the CT state, at least in the ultrafast time scale, is mainly ruled by the energy gap between CT and bright states. This gap, in turn, is determined by the electrostatic interactions with the surrounding solvent molecules, and we have observed remarkable differences in energy between the most and least stable configurations at the FC point of ~1 eV. It is therefore possible to conceive a fast computational route to predict the interplay between bright and CT states based on a limited number of 'computationally expensive' excited state dynamics simulations and large number of 'simple' electrostatic calculations. Of course, this simplified picture is expected to be valid only when intra-molecular vibrations have a limited effect on the inter-monomer electronic couplings. When this is not the case, especially when looking for a reliable description on a time scale $\geq$50 fs, an explicit treatment of the dynamical coupling between solute and solvent degrees of freedom is necessary, and we will proceed in this direction in future studies, tackling also the description of the PT reaction.

Acknowledgements

The authors thank Giacomo Prampolini (ICCOM-CNR), Javier Cerezo and Lara Martínez Fernandez (Universidad Autónoma de Madrid) for useful discussions. The support of the Joint Research Project (International Exchanges) CNR- Royal Society of London 2021–2022 is kindly acknowledged. FS and RI thank the CNR programs "Progetti di Ricerca @cnr", project UCATG4, and NUTRAGE for financial support. Open Access funding provided by Consiglio Nazionale delle Ricerche within the CRUI-CARE Agreement.

Conflict of Interest

The authors declare no conflict of interest.

Data Availability Statement

The data that support the findings of this study are available in the supplementary material of this article.

Keywords: Charge Transfer · Diabatic States · DNA · MCTDH · Photophysics

[1] R. Improta, F. Santoro, L. Blancafort, *Chem. Rev.* **2016**, *116*, 3540.
[2] C. T. Middleton, K. de La Harpe, C. Su, Y. K. Law, C. E. Crespo-Hernández, B. Kohler, *Annu. Rev. Phys. Chem.* **2009**, *60*, 217.
[3] D. Markovitsi, *Photochem. Photobiol.* **2016**, *92*, 45.
[4] W. Popp, D. Brey, R. Binder, I. Burghardt, *Annu. Rev. Phys. Chem.* **2021**, *72*, 591.
[5] L. Cupellini, D. Calvani, D. Jacquemin, B. Mennucci, *Nat. Commun.* **2020**, *11*, 662.
[6] C. Curutchet, B. Mennucci, *Chem. Rev.* **2017**, *117*, 294.
[7] T. Mirkovic, E. E. Ostroumov, J. M. Anna, R. van Grondelle, Govindjee, G. D. Scholes, *Chem. Rev.* **2017**, *117*, 249.
[8] N. J. Hestand, F. C. Spano, *Chem. Rev.* **2018**, *118*, 7069.
[9] X.-K. Chen, V. Coropceanu, J.-L. Brédas, *Nat. Commun.* **2018**, *9*, 5295.
[10] J. Lee, P. Jadhav, P. D. Reusswig, S. R. Yost, N. J. Thompson, D. N. Congreve, E. Hontz, T. Van Voorhis, M. A. Baldo, *Acc. Chem. Res.* **2013**, *46*, 1300.
[11] N. Monahan, X.-Y. Zhu, *Annu. Rev. Phys. Chem.* **2015**, *66*, 601.
[12] D. Casanova, *Chem. Rev.* **2018**, *118*, 7164.
[13] A. L. Sobolewski, W. Domcke, *Phys. Chem. Chem. Phys.* **2004**, *6*, 2763.
[14] A. L. Sobolewski, W. Domcke, C. Hättig, *Proc. Natl. Acad. Sci. USA* **2005**, *102*, 17903.
[15] L. Biemann, S. A. Kovalenko, K. Kleinermanns, R. Mahrwald, M. Markert, R. Improta, *J. Am. Chem. Soc.* **2011**, *133*, 19664.
[16] L. Martinez-Fernandez, R. Improta, *Faraday Discuss.* **2018**, *207*, 199.
[17] M. Barbatti, C. A. Borin, S. Ullrich, *Photoinduced Phenomena in Nucleic Acids I: Nucleobases in the Gas Phase and in Solvents*, volume 355, Springer International Publishing: Cham, Switzerland **2015**.
[18] R. Improta, T. Douki, *DNA Photodamage: From Light Absorption to Cellular Responses and Skin Cancer*, Royal Society of Chemistry **2021**.
[19] N. K. Schwalb, F. Temps, *J. Am. Chem. Soc.* **2007**, *129*, 9272.
[20] P. R. L. Markwick, N. L. Doltsinis, J. Schlitter, *The J. Chem. Phys* **2007**, *126*, 045104.
[21] P. R. L. Markwick, N. L. Doltsinis, *The J. Chem. Phys* **2007**, *126*, 175102.
[22] N. K. Schwalb, T. Michalak, F. Temps, *J. Phys. Chem. B* **2009**, *113*, 16365.
[23] K. Röttger, H. J. B. Marroux, M. P. Grubb, P. M. Coulter, H. Bohnke, A. S. Henderson, M. C. Galan, F. Temps, A. J. Orr-Ewing, G. M. Roberts, *Angew. Chem. Int. Ed.* **2015**, *54*, 14719.
[24] L. Martinez-Fernandez, G. Prampolini, J. Cerezo, Y. Liu, F. Santoro, R. Improta, *Chem. Phys.* **2018**, *515*, 493, ultrafast Photoinduced Processes in Poly- atomic Molecules:Electronic Structure, Dynamics and Spectroscopy (Dedicated to Wolfgang Domcke on the occasion of his 70th birthday).
[25] G. Groenhof, L. V. Schäfer, M. Boggio-Pasqua, M. Goette, H. Grubmüller, M. A. Robb, *J. Am. Chem. Soc.* **2007**, *129*, 6812.
[26] Y. Zhang, K. de La Harpe, A. A. Beckstead, R. Improta, B. Kohler, *J. Am. Chem. Soc.* **2015**, *137*, 7059.
[27] Y. Zhang, K. de La Harpe, A. A. Beckstead, L. Martínez-Fernández, R. Improta, B. Kohler, *J. Phys. Chem. Lett.* **2016**, *7*, 950.
[28] F. Santoro, J. A. Green, L. Martinez-Fernandez, J. Cerezo, R. Improta, *Phys. Chem. Chem. Phys.* **2021**, *23*, 8181.
[29] J. Cerezo, Y. Liu, N. Lin, X. Zhao, R. Improta, F. Santoro, *J. Chem. Theory Comput.* **2018**, *14*, 820.
[30] S. Thallmair, J. P. P. Zauleck, R. de Vivie-Riedle, *J. Chem. Theory Comput.* **2015**, *11*, 1987.
[31] S. Reiter, D. Keefer, R. de Vivie-Riedle, *J. Am. Chem. Soc.* **2018**, *140*, 8714.
[32] M. Pápai, M. Abedi, G. Levi, E. Biasin, M. M. Nielsen, K. B. Møller, *J. Phys. Chem. C* **2019**, *123*, 2056.

[33] A. Segalina, D. Aranda, J. A. Green, V. Cristino, S. Caramori, G. Prampolini, M. Pastore, F. Santoro, *J. Chem. Theory Comput.* **2022**, *18*, 3718, pMID: 35377648.
[34] J. Tomasi, B. Mennucci, R. Cammi, *Chem. Rev.* **2005**, *105*, 299..
[35] M. Caricato, B. Mennucci, J. Tomasi, F. Ingrosso, R. Cammi, S. Corni, G. Scalmani, *J. Chem. Phys.* **2006**, *124*, 124520.
[36] J. A. Green, M. Yaghoubi Jouybari, H. Asha, F. Santoro, R. Improta, *J. Chem. Theory Comput.* **2021**, *17*, 4660.
[37] M. Y. Jouybari, J. A. Green, R. Improta, F. Santoro, *J. Phys. Chem. A* **2021**, *125*, 8912.
[38] M. Beck, A. Jäckle, G. Worth, H.-D. Meyer, *Phys. Rep.* **2000**, *324*, 1 .
[39] F. Meyer, H.-D.and Gatti, G. A. Worth (Editors), *Mul- tidimensional Quantum Dynamics: MCTDH Theory and Applications*, Wiley-VCH, Weinheim **2009**.
[40] H. Wang, M. Thoss, *J. Chem. Phys.* **2003**, *119*, 1289.
[41] H. Wang, *J. Phys. Chem. A* **2015**, *119*, 7951.
[42] G. A. Worth, K. Giri, G. W. Richings, M. H. Beck, A. Jäckle, H.-D. Meyer, The QUANTICS Package, Version 1.1, (2015), University of Birmingham, Birmingham, U.K.
[43] G. Worth, *Comput. Phys. Commun.* **2020**, *248*, 107040.
[44] J. A. Green, H. Asha, F. Santoro, R. Improta, *J. Chem. Theory Comput.* **2021**, *17*, 405.
[45] M. Yaghoubi Jouybari, Y. Liu, R. Improta, F. Santoro, *J. Chem. Theory Comput.* **2020**, *16*, 5792.
[46] S. Corni, R. Cammi, B. Mennucci, J. Tomasi, *J. Chem. Phys.* **2005**, *123*, 134512.
[47] R. Cammi, S. Corni, B. Mennucci, J. Tomasi, *J. Chem. Phys.* **2005**, *122*, 104513.
[48] R. Improta, V. Barone, G. Scalmani, M. J. Frisch, *J. Chem. Phys.* **2006**, *125*, 054103.
[49] A. Segalina, J. Cerezo, G. Prampolini, F. Santoro, M. Pastore, *J. Chem. Theory Comput.* **2020**, *16*, 7061.
[50] J. Cerezo, D. Aranda, F. J. Avila Ferrer, G. Prampolini, F. Santoro, *J. Chem. Theory Comput.* **2020**, *16*, 1215.
[51] M. J. Frisch, G. W. Trucks, H. B. Schlegel, G. E. Scuseria, M. A. Robb, J. R. Cheeseman, G. Scalmani, V. Barone, G. A. Petersson, H. Nakatsuji, X. Li, M. Caricato, A. V. Marenich, J. Bloino, B. G. Janesko, R. Gomperts, B. Mennucci, H. P. Hratchian, J. V. Ortiz, A. F. Izmaylov, J. L. Sonnenberg, D. Williams-Young, F. Ding, F. Lipparini, F. Egidi, J. Goings, B. Peng, A. Petrone, T. Henderson, D. Ranasinghe, V. G. Zakrzewski, J. Gao, N. Rega, G. Zheng, W. Liang, M. Hada, M. Ehara, K. Toyota, R. Fukuda, J. Hasegawa, M. Ishida, T. Nakajima, Y. Honda, O. Kitao, H. Nakai, T. Vreven, K. Throssell, J. A. Montgomery Jr., J. E. Peralta, F. Ogliaro, M. J. Bearpark, J. J. Heyd, E. N. Brothers, K. N. Kudin, V. N. Staroverov, T. A. Keith, R. Kobayashi, J. Normand, K. Raghavachari, A. P. Rendell, J. C. Burant, S. S. Iyengar, J. Tomasi, M. Cossi, J. M. Millam, M. Klene, C. Adamo, R. Cammi, J. W. Ochterski, R. L. Martin, K. Morokuma, O. Farkas, J. B. Foresman, D. J. Fox, Gaussian 16 Revision B.01 **2016**, gaussian Inc. Wallingford CT.
[52] T. Yanai, D. Tew, N. Handy, *Chem. Phys. Lett.* **2004**, *393*, 51.
[53] J. A. Green, R. Improta, *Phys. Chem. Chem. Phys.* **2020**, *22*, 5509.
[54] M. L. Horng, J. A. Gardecki, A. Papazyan, M. Maroncelli, *J. Phys. Chem.* **1995**, *99*, 17311.
[55] C. I. Bayly, P. Cieplak, W. Cornell, P. A. Kollman, *J. Phys. Chem.* **1993**, *97*, 10269.
[56] D. Aranda, F. Santoro, *J. Chem. Theory Comput.* **2021**, *17*, 1691.
[57] J. A. Green, M. Yaghoubi Jouybari, D. Aranda, R. Improta, F. Santoro, *Molecules* **2021**, *26*, 1743.
[58] B. F. E. Curchod, T. J. Martínez, *Chemical Reviews* **2018**, *118*, 3305.
[59] R. Improta, *Phys. Chem. Chem. Phys.* **2008**, *10*, 2656.
[60] C. A. Guido, M. Rosa, R. Cammi, S. Corni, *J. Chem. Phys.* **2020**, *152*, 174114.
[61] G. D'Avino, L. Muccioli, C. Zannoni, D. Beljonne, Z. G. Soos, *J. Chem. Theory Comput.* **2014**, *10*, 4959.
[62] G. D'Avino, R. Hegger, D. Brey, P. K. Budakoti, S. Méry, I. Burghardt, *J. Phys. Chem. C* **2022**, *126*, 9762.
[63] L. P. Candeias, S. Steenken, *J. Am. Chem. Soc.* **1989**, *111*, 1094.
[64] L. P. Candeias, S. Steenken, *J. Am. Chem. Soc.* **1992**, *114*, 699.
[65] A. Banyasz, L. Martínez-Fernández, R. Improta, T.-M. Ketola, C. Balty, D. Markovitsi, *Phys. Chem. Chem. Phys.* **2018**, *20*, 21381.
[66] S. Thallmair, M. Kowalewski, J. P. P. Zauleck, M. K. Roos, R. de Vivie-Riedle, *J. Phys. Chem. Lett.* **2014**, *5*, 3480.
[67] J. P. P. Zauleck, M. T. Peschel, F. Rott, S. Thallmair, R. de Vivie-Riedle, *J. Phys. Chem. A* **2018**, *122*, 2849.
[68] R. Improta, G. Scalmani, M. J. Frisch, V. Barone, *J. Chem. Phys.* **2007**, *127*, 074504.
[69] M. Bondanza, M. Nottoli, L. Cupellini, F. Lipparini, B. Mennucci, *Phys. Chem. Chem. Phys.* **2020**, *22*, 14433.
[70] A. J. Dunnett, D. Gowland, C. M. Isborn, A. W. Chin, T. J. Zuehlsdorff, *The J. Chem. Phys* **2021**, *155*, 144112.
[71] T. M. Clarke, J. R. Durrant, *Chem. Rev.* **2010**, *110*, 6736.

Manuscript received: June 6, 2022
Accepted manuscript online: August 11, 2022
Version of record online: October 7, 2022